JACS
JOURNAL OF THE AMERICAN CHEMICAL SOCIETY

Article

pubs.acs.org/JACS

Near Infrared Light-Powered Janus Mesoporous Silica Nanoparticle Motors

Mingjun Xuan,[†,§] Zhiguang Wu,[†,§] Jingxin Shao,[†] Luru Dai,[‡] Tieyan Si,*[,†] and Qiang He*[,†]

[†]State Key Laboratory of Robotics and System (HIT), Micro/Nanotechnology Research Centre, Harbin Institute of Technology, Harbin 150080, China

[‡]CAS Key Lab for Biomedical Effects of Nanomaterials and Nanosafety, National Center for Nanoscience and Technology, Beijing 100190, China

Supporting Information

ABSTRACT: We describe fuel-free, near-infrared (NIR)-driven Janus mesoporous silica nanoparticle motors (JMSNMs) with diameters of 50, 80, and 120 nm. The Janus structure of the JMSNMs is generated by vacuum sputtering of a 10 nm Au layer on one side of the MSNMs. Upon exposure to an NIR laser, a localized photothermal effect on the Au half-shells results in the formation of thermal gradients across the JMSNMs; thus, the generated self-thermophoresis can actively drive the nanomotors to move at an ultrafast speed, for instance, up to 950 body lengths/s for 50 nm JMSNMs under an NIR laser power of 70.3 W/cm^2. The reversible "on/off" motion of the JMSNMs and their directed movement along the light gradient can be conveniently modulated by a remote NIR laser. Moreover, dynamic light scattering measurements are performed to investigate the coexisting translational and rotational motion of the JMSNMs in the presence of both self-thermophoretic forces and strong Brownian forces. These NIR-powered nanomotors demonstrate a novel strategy for overcoming the necessity of chemical fuels and exhibit a significant improvement in the maneuverability of nanomotors while providing potential cargo transportation in a biofriendly manner.

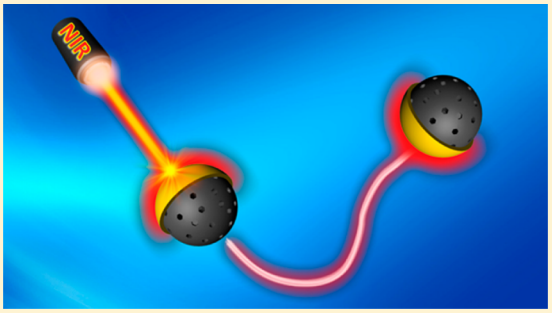

INTRODUCTION

Since the appearance of chemically powered self-propelled nanomotors, motor-based active transportation has been demonstrated to perform various complex tasks in fluids.[1−12] Polymer-based nanomotors constructed using "bottom-up" self-assembly approaches integrate self-driven navigation capabilities;[13−17] thus, they can achieve not only smart encapsulation and release but also precise guidance and control,[18−21] with potential in the design of new-generation drug-delivery vehicles.[22,23] Additionally, recent research has revealed that vehicle size plays a key role in the circulation time and biodistribution of nanoparticles in living organisms; drug carriers with diameters of less than 200 nm achieve a longer circulation time in blood, with a reduced possibility of the drug being cleared by the immune system.[24] In previous reports, researchers have synthesized several sub-100 nm artificial motors, including platinum (Pt)-modified mesoporous silica nanoparticle motors (MSNMs) and Pt−Au Janus motors,[25−34] but these motors were powered by the catalytic decomposition of toxic hydrogen peroxide fuels. Recently, fuel-free synthetic motors propelled by external physical stimuli, including magnetic fields,[35−37] electric fields,[38] ultrasonic waves,[39,40] and light,[41−45] have been investigated because they can overcome the limitation caused by using chemical fuels (i.e., H_2O_2) and allow for remote intervention in terms of the direction and speed of the motion, as well as the "on/off" states in a controlled manner, which is of great importance in biomedical applications. Nevertheless, the design of fuel-free self-driven nanomotors that can achieve cargo loading and release in a precisely directed manner is still challenging.

Mesoporous silica nanoparticles (MSNs) have been widely reported as a theranostic platform in the biomedical field due to their high cargo-loading capacity and superior biocompatibility.[46−48] Gold nanoshells (AuNSs) are known to generate heat under near-infrared (NIR) irradiation due to their surface plasmon resonance (SPR) band and thus have exhibited NIR-triggered photothermal therapy, drug release, and imaging functions.[49,50] NIR light is an especially attractive stimulus due to its ability to penetrate tissue with minimal absorption and its ease of localized stimulus application.[51] Herein, we report AuNS-functionalized Janus MSN motors (JMSNMs) with tunable sizes (50, 80, and 120 nm) and demonstrate their NIR-driven swimming behavior in water due to the photothermal effect of the AuNSs. NIR-driven JMSNMs can move rapidly in water, and their on/off propulsion can be easily modulated via NIR laser illumination. Given the presence of strong Brownian forces, we conduct a systemic investigation on their NIR-driven motion, including translational and rotational Brownian diffusion, by dynamic light scattering (DLS). The

Received: January 26, 2016
Published: May 6, 2016

DOI: 10.1021/jacs.6b00902
J. Am. Chem. Soc. 2016, 138, 6492−6497

observed rapid rotational Brownian diffusion has little effect on the high-speed motion of the JMSNMs upon exposure to an NIR laser. Such NIR-driven nanomotors combining the advantages of both MSNs and NIR light provide an alternative strategy for biofriendly motion-based drug delivery and other biomedical applications.

RESULTS AND DISCUSSION

MSNs with different sizes were first synthesized by the traditional "sol–gel" process, as reported in the literature.[52] The scanning electron microscopy (SEM) and transmission electron microscopy (TEM) images presented in Figure S1 [see Supporting Information (SI)] show that the as-synthesized MSNs with 2–3 nm ordered pore channels were monodispersed, with sizes of 50, 80, and 120 nm. Next, the MSNs were spread on a silicon slide to form a two-dimensional MSN monolayer; the MSNs were subsequently coated with a 10 nm Au layer, and then the Au-functionalized Janus MSNMs were released and suspended in water, as shown in Figure 1a. The

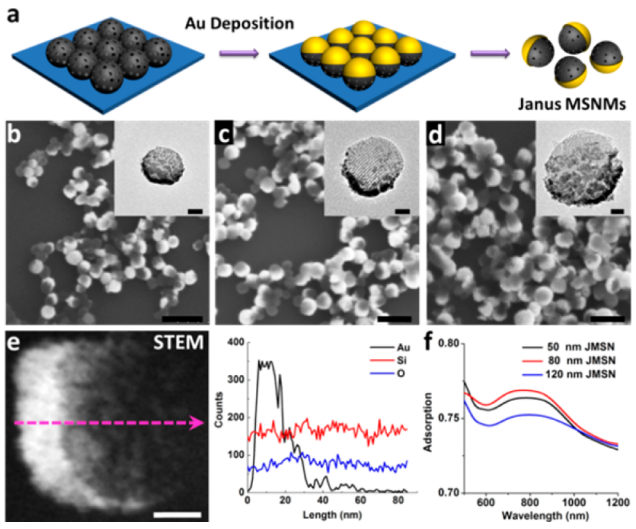

Figure 1. Characterization of the AuNS-modified JMSNMs. (a) Fabrication scheme of the JMSNMs. (b–d) SEM images of JMSNMs with diameters of 50, 80, and 120 nm. Scale bar = 200 nm. The insets display corresponding TEM images. Scale bar = 20 nm. (e) STEM image of an 80 nm JMSMN and corresponding EDX spectra for the distribution of Au, Si, and O elements. Scale bar = 20 nm. (f) UV–vis–NIR spectra of the JMSNMs.

SEM images in Figure 1b–d show the formation of clear Janus structures for all three sizes of MSNMs, with Au layers shown as a bright color. The inset TEM images confirm the ordered porous channels of the uncoated side of the JMSNMs. The scanning transmission electron microscopy (STEM) image and corresponding energy-dispersive X-ray (EDX) spectra of selected 80 nm JMSNMs shown in Figure 1e illustrate the asymmetric distribution of Au, suggesting the successful deposition of AuNSs on one side of the JMSNMs. In addition, the UV–vis–NIR spectra of the JMSNMs in Figure 1f reveal the maximum SPR peak of the AuNSs at approximately 800 nm, which is important for the photothermal conversion effect in the NIR region. In contrast, no adsorption peaks were detected in the UV–vis-NIR spectra of the MSNMs (Figure S2).

Two-photon confocal laser scanning microscopy (TP-CLSM) employing an 808 nm fiber-coupled femtosecond laser was conducted to supply an NIR light source and to record the trajectory of the JMSNMs. JMSNMs with varying diameters were first labeled with fluorescein isothiocyanate (FITC) to allow their motion to be observed by TP-CLSM in fluorescence mode (Figure S3). The time-lapse images shown in Figure 2a, captured from videos 1, 2, and 3 (Supporting

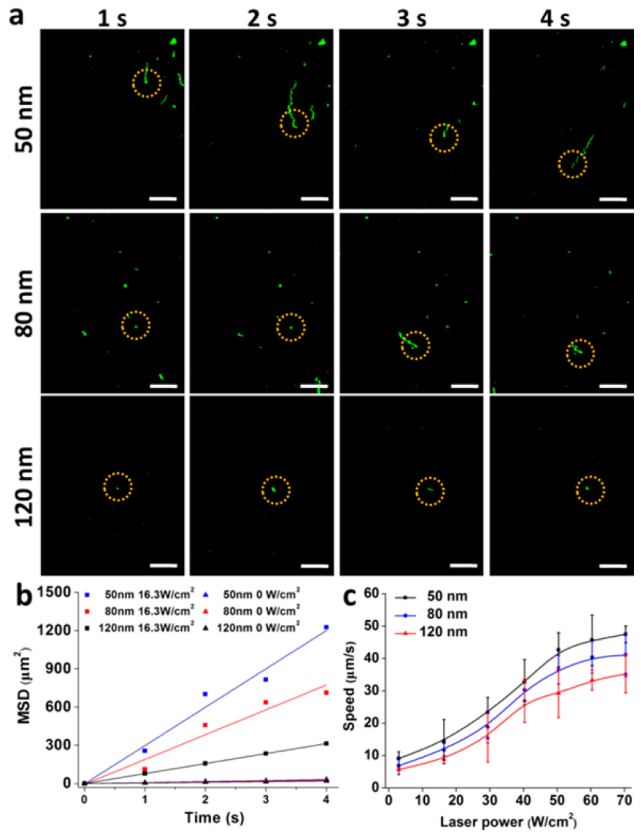

Figure 2. JMSNM motion analysis results. (a) Time-lapsed images of JMSNMs with diameters of 50, 80, and 120 nm under exposure to an NIR laser at 16.3 W/cm^2. Scale bar = 20 μm. (b) The mean motion displacement of JMSNMs at an NIR power of 16.3 W/cm^2 in 4 s. (c) The speed distribution of JMSNMs under exposure to variable NIR powers.

Information), illustrate the rapid propulsion of the JMSNMs with diameters of 50, 80, and 120 nm under NIR irradiation at a power of 16.3 W/cm^2. Note that the presence of the green tails is caused by the low scanning rate of the TP-CLSM, reflecting the motion trajectory of the JMSNMs, but the difference in the length of the green tails should be ascribed to the fact that most of the nanomotors did not move in the same confocal plane during the scanning period. Moreover, the photothermal conversion effect occurs only on the Au-coated side, and thus the nanomotor should swim opposite to the direction of the Au half-shell side. Figure 2b displays the mean squared displacement (MSD) for the three different JMSNM sizes as a function of time without and with NIR irradiation (16.3 W/cm^2). As a result, the average speeds of the 50, 80, and 120 nm JMSNMs were 17.8, 11.8, and 8.1 μm/s, respectively, which correspond to relative speeds of nearly 356, 148, and 68 body lengths/s, respectively. Obviously, the smaller JMSNMs swam faster under the same conditions. This result is ascribed to the fact that although the larger JMSNM produces more heat due to its larger Au surface area, the local temperature gradient generated

DOI: 10.1021/jacs.6b00902
J. Am. Chem. Soc. 2016, 138, 6492–6497

across the larger JMSNM is much weaker than that across the smaller nanomotors due to the finite size effect; additionally, the larger particle encounters greater resistance in the fluid. In the control experiments, the JMSNMs did not show any significant visible movement in the absence of NIR irradiation (Figure S4, SI videos 4–6), and similarly, both optical microscopy images (Figure S5) and MSD calculations (Figure S6) confirm that bare MSNs without Au deposition exhibited only normal Brownian motion under irradiation of a 16.3 W/cm^2 NIR laser. Figure S7 shows that the Au whole-shell coated MSNs (AuWS-MSNs) with a symmetric structure exhibited Brownian motion under irradiation of the 16.3 W/cm^2 NIR laser. Figure S8 shows that the diffusion coefficients of the bare MSNs, AuWS-MSNs, and JMSNMs are 2.5 × 10^{-12}, 10.4 × 10^{-12}, and 44.5 × 10^{-12} m^2/s, respectively. Note that the motion of the bare MSNs was independent of the NIR irradiation and that the motion of the AuWS-MSNs improved slightly due to the increased temperature in the presence of NIR light. Furthermore, Figure S9 shows that the measured diffusion coefficients of the symmetric AuWS-MSNs at four different temperatures without NIR irradiation are almost identical to the theoretically computed values. These results demonstrate that the rapid increase in temperature did not generate a strong convective current in our system. Subsequently, an NIR laser with variable power (0–70 W/cm^2) was used to illuminate the JMSNMs because the NIR laser intensity is expected to modulate the speed of the JMSNMs. It can be observed that the speed for the three JMSNM sizes increasingly rises with increasing NIR laser power (Figure 2c). Note that the nonlinear dependency between the speed of the JMSNMs and the NIR laser intensity is partly caused by the shift of the maximum absorption peak due to melting and deformation of the Au half-shell surface with increased local temperature.[53] Finally, we also tested the movement of these NIR-driven JMSNMs in phosphate buffer solution (PBS) and fetal bovine serum (FBS). The selected 80 nm JMSNMs could effectively perform self-propulsion motion in PBS (5.86 μm/s) and FBS (1.76 μm/s) upon exposure to a 3 W/cm^2 NIR laser, as shown in Figure S10. The decreased speed in the FBS is ascribed to the higher viscosity and the heat diffusion of proteins in the vicinity of the Au half-shells.[54]

The speed of the JMSNMs could be easily regulated by tuning the power of the NIR laser. The "on/off" motion of these JMSNMs could likewise be controlled by the "open/close" NIR light source. To investigate this phenomenon, the 80 nm JMSNMs were selected as an example. The time-lapsed microscopic images displayed in Figure 3a, taken from video 7 (Supporting Information), illustrate reversible and rapid stopping and starting of the artificial nanomotors as the NIR laser was switched on/off. In the absence of NIR illumination, three of the 80 nm JMSNMs show Brownian motion, which can be thought of as a "stop" state, before 26 s. Upon exposure to the 3 W/cm^2 NIR laser at 26 s, the expected displacement was immediately observed for the three indicated motors.

Once the NIR laser is switched off at 37 s, the nanomotors rapidly decelerated and completely stopped their motion (Figure 3a). The change in speed of the JMSNMs during two "off/on/off" cycles corresponds to an average speed of approximately 6.43 μm/s during NIR irradiation (Figure 3b). The cyclic "on/off" NIR activation of the nanomotor motion can be repeated, which indicates great promise for on-demand regulation of the motion of fuel-free JMSNMs by an external "on/off" NIR laser switch.

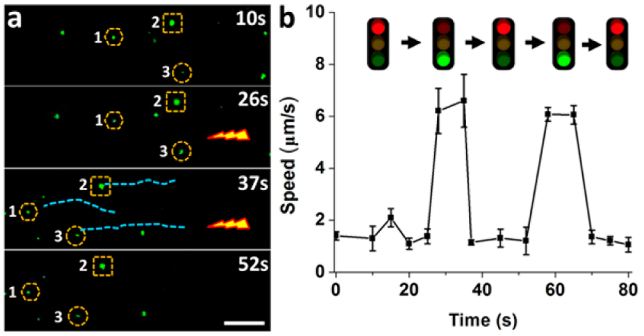

Figure 3. Time-lapsed microscopic images of the "on/off" motion of 80 nm JMSNMs triggered by a 3 W/cm^2 NIR laser (a) and the corresponding speed–time dependence (b). Scale bar = 20 μm.

Due to the SPR absorption of the AuNSs in the NIR region, the half-capped AuNSs on the JMSNMs convert the adsorbed photons to heat; thus, the hot AuNSs act as a heating source and generate local thermal gradients across the JMSNMs. The temperature of the JMSNM suspension, recorded by a sensitive electric coupling thermometer, showed a rapid increase under NIR irradiation at 3.0 W/cm^2 and eventually reached a plateau within 7 min (Figure 4a). The rate of the temperature increase

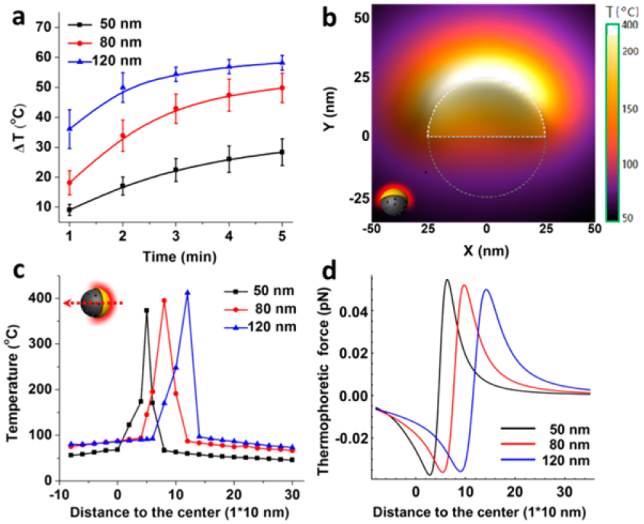

Figure 4. Theoretical simulation of self-thermophoretic propulsion of JMSNMs at a constant laser power (3.0 W/cm^2). (a) The measured rate of temperature rise and the final temperature were proportional to the nanomotor size. (b) The steady-state temperature distribution for a 50 nm JMSNM under 3 W/cm^2 NIR irradiation. (c) The computed temperature distribution along the central line perpendicular to the interfacial plane between the AuNS and MSN hemispheres. (d) The self-thermophoretic force calculated from the local temperature gradient.

and the final temperature were proportional to the nanomotor sizes and the laser power. Here, the NIR light provides a steady input of thermal energy, although some of the thermal energy is dissipated into the water. When the input and dissipation reach a balance, the solution achieves a steady state for which the thermal diffusion equation can be used to give an approximate theoretical description. According to the thermal diffusion equation, the temperature increase in the vicinity of the AuNSs is proportional to the particle volume, $T = VQ/4\pi kr$ (V, JMSNM volume; Q, energy from the light; k, thermal

DOI: 10.1021/jacs.6b00902
J. Am. Chem. Soc. 2016, 138, 6492–6497

conductivity of the surrounding medium; r, radius).[55] The volume of the AuNS can be calculated by $V = 4\pi r^2 d/2$ (d, thickness of the AuNS; r, radius of the JMSNM), and the volume of the JMSNM is approximately equal to that of a solid ball particle whose radius is $R = (3r^2 d/2)^{1/3}$. In the steady state, the temperature profile around the JMSNMs can be numerically fit by $T(r) = A + B/r$.[56]

Figure 4b shows the profile of the temperature increase for a 50 nm JMSNM under 3 W/cm^2 NIR irradiation, which exhibits a sudden temperature increase at the interface between the motor and the water. The theoretically computed temperature distribution is also displayed along the central line perpendicular to the interfacial plane between the AuNS and MSN hemispheres (Figure 4c). Assuming that the thermal conductances of the JMSNMs with three diameters are identical, the estimated sudden temperature increase at the boundary is approximately 300 °C. Here, the experimentally measured temperature at 260 nm was taken as an initial value for the theoretical computation. A sudden divergence of temperature occurs exactly at the position of the AuNSs, crossing the boundary at 50, 80, and 120 nm. Furthermore, the thermophoretic force exerted on the JMSNMs can be estimated by the equation $F_Z = -C\partial_Z T$, where the coefficient $C = (9\pi d_p \eta^2 k_a)/(2\rho_g T k_p)$ (d_p, JMSNM diameter; η, fluid viscosity; k_a, fluid thermal conductivity; ρ_g, fluid density; k_p, thermal conductivity of the JMSNM).[57] Here, the thermophoretic force is proportional to the local temperature gradient and the JMSNM diameter. Figure 4d shows the distribution of thermophoretic forces along the central line of the JMSNMs, which is perpendicular to the boundary region between the AuNS and MSN hemispheres. Assuming that the thermophoretic force inside the AuNSs is a negative propulsion force, the thermophoretic force outside is thus positive. The positive propulsion force is apparently larger than the in-shell force vectors. As a result, the JMSNMs can be propelled into the direction along the MSN hemisphere. Therefore, the net propulsion forces on the 50, 80, and 120 nm JMSNMs are estimated to be 0.057, 0.052, and 0.049 pN, respectively, from Figure 4d; these forces are similar to the drag forces (0.051, 0.050, and 0.046 pN, respectively) calculated by Stokes' equation, $F_d = 6\pi\eta r v$, where F_d is the fluid resistance, v is the speed of the motor, η is the fluid viscosity, and r is the radius. Because the generated temperature gradient across smaller particles is stronger than that across larger particles, the thermophoretic force dominated by the temperature gradient on a smaller motor is larger than that exerted on a larger motor. This explanation is in accordance with the experimental results shown in Figure 2. Our theoretical computation demonstrates that the propulsion force of the JMSNMs primarily arises from the thermophoretic force on the JMSNMs upon exposure to an NIR laser; thus, the NIR-driven JMSNM motion is attributed to a self-thermophoresis mechanism.

We employed TP-CLSM to record the motion of the JMSNMs in fluorescence mode, but TP-CLSM is not sufficiently sensitive to investigate such small nanomotors in the presence of strong Brownian motion; thus, dynamic light scattering (DLS) equipped with a fiber-coupled diode laser was utilized. The rotational diffusion relaxation time of the ellipsoidal JMSNMs can be directly measured, and the obtained data were approximated according to the method recently described by Fischer et al.[25] Figure 5a shows that the observed rotational diffusion relaxation times of the 50, 80, and 120 nm JMSNMs in water in the absence of the NIR laser are 79, 102,

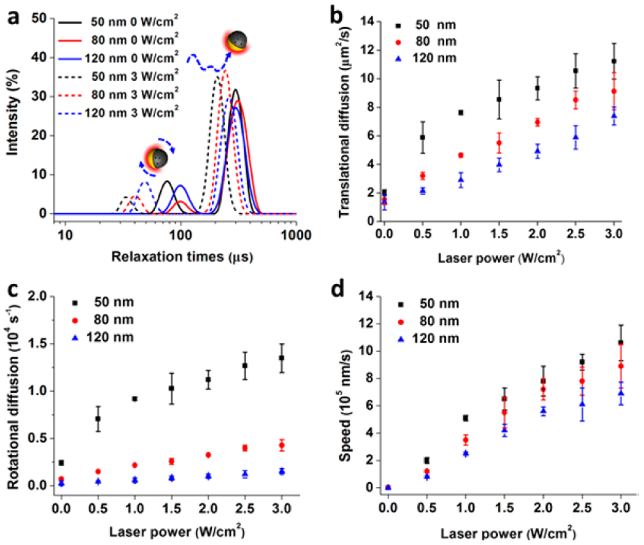

Figure 5. DLS characterization of NIR-driven JMSNMs in water. (a) Translational and rotational relaxation plots of the 50, 80, and 120 nm JMSNMs without and with NIR irradiation at 3 W/cm^2. The translational (b) and rotational (c) diffusion coefficients for the three JMSNM sizes at different levels of NIR irradiation power in water. (d) The computed average speed of JMSNMs between rotations at different levels of NIR irradiation power.

and 111 μs, respectively. These values correspond to theoretical rotational relaxation times of 65, 90, and 106 μs for 50, 80, and 120 nm spheres, respectively, in water, based on Stokes' equation for rotational Brownian motion. Upon exposure to the NIR laser at 3 W/cm^2, a significant shift in the relaxation peaks for the 50, 80, and 120 nm JMSNMs was observed; thus, the corresponding rotational relaxation times decreased to 33, 38, and 51 μs, respectively. Meanwhile, the translational relaxation times of the 50, 80, and 120 nm JMSNMs were 276, 342, and 396 μs for Brownian motion; these values decreased to 190, 230, and 295 μs in water with NIR irradiation at 3 W/cm^2, respectively. This finding suggests that NIR irradiation improves the JMSNM navigation ability in the presence of Brownian motion.

Moreover, one can observe that both the translational and rotational diffusion coefficients for the three JMSNM sizes show a significant increase with increasing NIR irradiation power (0−3 W/cm^2) (Figure 5b,c). Interestingly, the smaller JMSNMs displayed a greater increase in diffusion coefficients for a given NIR irradiation power, particularly for the rotational diffusion coefficient. Finally, the average speed can be acquired from the following equation: $D_T = D_0 + V^2\tau/4$, where D_T is the apparent translational diffusion coefficient under NIR exposure, D_0 is the translational diffusion coefficient without NIR irradiation, and τ is the rotation relaxation time.[58] The computed results displayed in Figure 5d indicate that the average speed of the JMSNMs increases linearly with increasing NIR irradiation power (0−3 W/cm^2), which is in agreement with the results obtained from the TP-CLSM observations shown in Figure 2c. Taken together, we find that the relaxation times decrease with increasing NIR irradiation power, but that the average speed of the JMSNMs increases with increasing laser power.

Previous studies have demonstrated that chemically catalytic mesoporous silica nanomotors have a high loading capacity because of their exceptionally high surface area for diverse

DOI: 10.1021/jacs.6b00902
J. Am. Chem. Soc. 2016, 138, 6492−6497

cargoes and cargo combinations.[40] To evaluate their capability for NIR-driven transportation, FITC-loaded JMSNMs were initially placed in the left-side reservoir of a microfluidic chip comprising two reservoirs that were associated by a channel, and an NIR light source was placed opposite the left-side reservoir, as shown in Figure 6a. In the absence of NIR light,

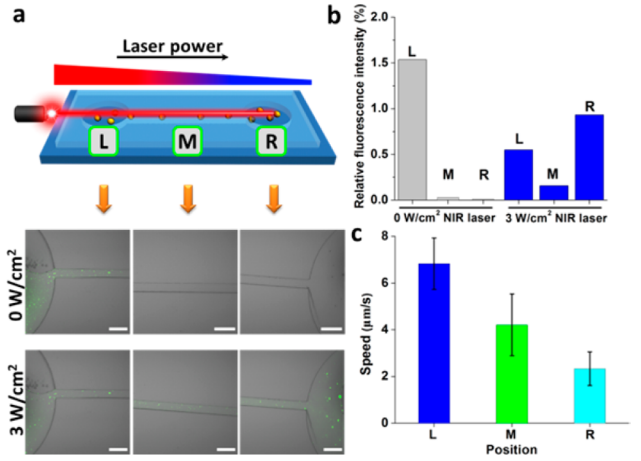

Figure 6. (a) Schematic illustration of on-chip cargo delivery by the 80 nm JMSNMs (top) and TP-CLSM images (bottom) of actively diffusing FITC-loaded JMSNMs in different positions with and without gradient NIR laser irradiation; scale bar = 200 μm. (b) Relative fluorescence intensity of FITC-loaded JMSNMs located at three positions before and after NIR light irradiation. (c) The average speed of the JMSNMs at different points along the NIR gradient.

most of the JMSNMs remained in the left-side reservoir due to their low diffusion rate; meanwhile, no green fluorescence dots were observed in either the channel or the right-side reservoir. Upon 3 W/cm^2 NIR light irradiation, many moving green fluorescence dots were observed in both the channel and the right-side reservoir, suggesting NIR-triggered active diffusion of the nanomotors toward the targeted right-side reservoir with the use of light irradiation for remote guidance.

The relative fluorescence intensity of three positions was quantified using ImageJ software (Figure 6b). The numbers of nanomotors in the voyage channel and in the left micro-reservoir show a prominent increase. The speed distribution was also observed (Figure 6c); the nanomotors with a lower speed (2.33 μm/s) accumulated at position R, indicating that a low laser power provides a more stable field for maintaining the nanomotors in a given position.

CONCLUSIONS

In conclusion, we successfully fabricated fuel-free, NIR-propelled, AuNS-functionalized Janus mesoporous silica nanoparticle motors (JMSNMs) with a tunable nanosize. Due to the strong SPR absorption of the AuNSs in the NIR region, thermophoretic forces along the asymmetric structure of the JMSNMs produce a net resultant force, which, in turn, can overcome strong Brownian forces and thus induce rapid motion of the nanomotors, as demonstrated experimentally and theoretically. We can conveniently modulate the speed of the JMSNMs by tuning the NIR light power and can also start and stop the motion of the JMSNMs on demand by switching the NIR laser. Such NIR-propelled nanomotors with a high loading capacity can provide a method for novel fuel-free propulsion and control of synthetic nanomachines in a biocompatible manner and thus pave the way for developing robust next-generation delivery nanovehicles for biomedical applications.

ASSOCIATED CONTENT

Supporting Information

The Supporting Information is available free of charge on the ACS Publications website at DOI: 10.1021/jacs.6b00902.

Descriptions of materials, equipment, and experimental procedures (PDF)
Motion movie of 50 nm JMSNMs upon the 16.3 W/cm^2 NIR light (AVI)
Motion movie of 80 nm JMSNMs upon the 16.3 W/cm^2 NIR light (AVI)
Motion movie of 120 nm JMSNMs upon the 16.3 W/cm^2 NIR light (AVI)
In the absence of NIR light, the Brownian motions of 50 nm JMSNMs (AVI)
In the absence of NIR light, the Brownian motions of 80 nm JMSNMs (AVI)
In the absence of NIR light, the Brownian motions of 120 nm JMSNMs (AVI)
Power "on/off" motion of 80 nm JMSNMs upon 3 W/cm^2 NIR light (AVI)

AUTHOR INFORMATION

Corresponding Authors

*tieyansi@hit.edu.cn
*qianghe@hit.edu.cn

Author Contributions

§M. X. and Z. W. contributed equally.

Notes

The authors declare no competing financial interest.

ACKNOWLEDGMENTS

We acknowledge Prof. Junbai Li for discussion. This work was supported by the National Nature Science Foundation of China (21573053, 21273053), National Key Foundation for Exploring Scientific Instrument (2013YQ16055108), and State Key Laboratory of Robotics and System (HIT).

REFERENCES

(1) Wang, J. *Nanomachines: Fundamentals and Applications*; Wiley-VCH: Weinheim, 2013.
(2) Palacci, J.; Sacanna, S.; Steinberg, A. P.; Pine, D. J.; Chaikin, P. M. *Science* **2013**, *339*, 936.
(3) Wilson, D. A.; Nolte, R. J. M.; van Hest, J. C. M. *Nat. Chem.* **2012**, *4*, 268.
(4) Gao, W.; Wang, J. *ACS Nano* **2014**, *8*, 3170.
(5) Ozin, G. A.; Manners, I.; Fournier-Bidoz, S.; Arsenault, A. *Adv. Mater.* **2005**, *17*, 3011.
(6) Mei, Y.; Solovev, A. A.; Sánchez, S.; Schmidt, O. G. *Chem. Soc. Rev.* **2011**, *40*, 2109.
(7) Wang, W.; Duan, W.; Ahmed, S.; Sen, A.; Mallouk, T. E. *Acc. Chem. Res.* **2015**, *48*, 1938.
(8) Sánchez, S.; Soler, L.; Katuri, J. *Angew. Chem., Int. Ed.* **2015**, *54*, 1414.
(9) Paxton, W. F.; Kistler, K. C.; Olmeda, C. C.; Sen, A.; St. Angelo, S. K.; Cao, Y.; Mallouk, T. E.; Lammert, P. E.; Crespi, V. H. *J. Am. Chem. Soc.* **2004**, *126*, 13424.
(10) Guix, M.; Mayorga-Martinez, C. C.; Merkoçi, A. *Chem. Rev.* **2014**, *114*, 6285.
(11) Wang, H.; Pumera, M. *Chem. Rev.* **2015**, *115*, 8704.
(12) Ghosh, A.; Fischer, P. *Nano Lett.* **2009**, *9*, 2243.

DOI: 10.1021/jacs.6b00902
J. Am. Chem. Soc. 2016, 138, 6492−6497

(13) Zhang, L.; Abbott, J. J.; Dong, L.; Peyer, K. E.; Kratochvil, B. E.; Zhang, H.; Bergeles, C.; Nelson, B. J. *Nano Lett.* **2009**, *9*, 3663.
(14) Gao, W.; Sattayasamitsathit, S.; Orozco, J.; Wang, J. *J. Am. Chem. Soc.* **2011**, *133*, 11862.
(15) Gao, W.; Uygun, A.; Wang, J. *J. Am. Chem. Soc.* **2012**, *134*, 897.
(16) Sánchez, S.; Solovev, A. A.; Mei, Y.; Schmidt, O. G. *J. Am. Chem. Soc.* **2010**, *132*, 13144.
(17) Dong, B.; Zhou, T.; Zhang, H.; Li, C. Y. *ACS Nano* **2013**, *7*, 5192.
(18) Qiu, T.; Lee, T.; Mark, A. G.; Morozov, K. I.; Münster, R.; Mierka, O.; Turek, S.; Leshansky, A. M.; Fischer, P. *Nat. Commun.* **2014**, *5*, 5119.
(19) Wang, W.; Chiang, T.-Y.; Velegol, D.; Mallouk, T. E. *J. Am. Chem. Soc.* **2013**, *135*, 10557.
(20) Mou, F.; Chen, C.; Ma, H.; Yin, Y.; Wu, Q.; Guan, J. *Angew. Chem., Int. Ed.* **2013**, *52*, 7208.
(21) Wang, H.; Zhao, G.; Pumera, M. *J. Am. Chem. Soc.* **2014**, *136*, 2719.
(22) Chałupniak, A.; Morales-Narváez, E.; Merkoçi, A. *Adv. Drug Delivery Rev.* **2015**, *95*, 104.
(23) Lin, X.; Wu, Z.; Wu, Y.; Xuan, M.; He, Q. *Adv. Mater.* **2016**, *28*, 1060.
(24) Hu, C. M.; Fang, R.; Copp, J.; Luk, B.; Zhang, L. *Nat. Nanotechnol.* **2013**, *8*, 336.
(25) Lee, T.; Alarcón-Correa, M.; Miksch, C.; Hahn, K.; Gibbs, J. G.; Fischer, P. *Nano Lett.* **2014**, *14*, 2407.
(26) Lal, S.; Clare, S. E.; Halas, N. J. *Acc. Chem. Res.* **2008**, *41*, 1842.
(27) Ma, X.; Hahn, K.; Sánchez, S. *J. Am. Chem. Soc.* **2015**, *137*, 4976.
(28) Jiang, H.; Yoshinaga, N.; Sano, M. *Phys. Rev. Lett.* **2010**, *105*, 268302.
(29) Ma, X.; Jannasch, A.; Albrecht, U.; Hahn, K.; Miguel-López, A.; Schäffer, E.; Sánchez, S. *Nano Lett.* **2015**, *15*, 7043.
(30) Baraban, L.; Makarov, D.; Streubel, R.; Mönch, I.; Grimm, D.; Sánchez, S.; Schmidt, O. G. *ACS Nano* **2012**, *6*, 3383.
(31) Gao, W.; Pei, A.; Dong, R.; Wang, J. *J. Am. Chem. Soc.* **2014**, *136*, 2276.
(32) Wang, L.; Liu, Y.; He, J.; Hourwitz, M. J.; Yang, Y.; Fourkas, J. T.; Han, X.; Nie, Z. *Small* **2015**, *11*, 3762.
(33) Schattling, P.; Thingholm, B.; Städler, B. *Chem. Mater.* **2015**, *27*, 7412.
(34) Simmchen, J.; Baeza, A.; Ruiz, D.; Esplandiu, M. J.; Vallet-Regí, M. *Small* **2012**, *8*, 2053.
(35) Zhang, L.; Petit, T.; Lu, Y.; Kratochvil, B. E.; Peyer, K. E.; Pei, R.; Lou, J.; Nelson, B. J. *ACS Nano* **2010**, *4*, 6228.
(36) Cheng, R.; Huang, W.; Huang, L.; Yang, B.; Mao, L.; Jin, K.; ZhuGe, Q.; Zhao, Y. *ACS Nano* **2014**, *8*, 7746.
(37) Gao, W.; Sattayasamitsathit, S.; Manesh, K. M.; Weihs, D.; Wang, J. *J. Am. Chem. Soc.* **2010**, *132*, 14403.
(38) Paxton, W. F.; Baker, P. T.; Kline, T. R.; Wang, Y.; Mallouk, T. E.; Sen, A. *J. Am. Chem. Soc.* **2006**, *128*, 14881.
(39) Wang, W.; Luz Angelica, C.; Hoyos, M.; Mallouk, T. E. *ACS Nano* **2012**, *6*, 6122.
(40) Wu, Z.; Li, T.; Gao, W.; Xu, T.; Jurado-Sánchez, B.; Li, J.; Gao, W.; He, Q.; Zhang, L.; Wang, J. *Adv. Funct. Mater.* **2015**, *25*, 3881.
(41) Zong, Y.; Liu, J.; Liu, R.; Guo, H.; Yang, M.; Li, Z.; Chen, K. *ACS Nano* **2015**, *9*, 10844.
(42) Palacci, J.; Sacanna, S.; Vatchinsky, A.; Chaikin, P. M.; Pine, D. J. *J. Am. Chem. Soc.* **2013**, *135*, 15978.
(43) Shao, L.; Yang, Z.; Andren, D.; Johansson, P.; Käll, M. *ACS Nano* **2015**, *9*, 12542.
(44) Wu, Z.; Si, T.; Gao, W.; Lin, X.; Wang, J.; He, Q. *Small* **2016**, *12*, 577.
(45) Yamada, M.; Kondo, M.; Mamiya, J.-i.; Yu, Y.; Kinoshita, M.; Barrett, C. J.; Ikeda, T. *Angew. Chem., Int. Ed.* **2008**, *47*, 4986.
(46) Wan, Y.; Zhao, D. *Chem. Rev.* **2007**, *107*, 2821.
(47) Pan, L.; He, Q.; Liu, J.; Chen, Y.; Ma, M.; Zhang, L.; Shi, J. *J. Am. Chem. Soc.* **2012**, *134*, 5722.
(48) Hoffmann, F.; Cornelius, M.; Morell, J.; Fröba, M. *Angew. Chem., Int. Ed.* **2006**, *45*, 3216.
(49) Wang, H.; Brandl, D. W.; Le, F.; Nordlander, P.; Halas, N. J. *Nano Lett.* **2006**, *6*, 827.
(50) Huschka, R.; Zuloaga, J.; Knight, M. W.; Brown, L.; Nordlander, P.; Halas, N. J. *J. Am. Chem. Soc.* **2011**, *133*, 12247.
(51) Weissleder, R. *Nat. Biotechnol.* **2001**, *19*, 316.
(52) Xuan, M.; Shao, J.; Lin, X.; Dai, L.; He, Q. *ChemPhysChem* **2014**, *15*, 2255.
(53) Qin, Z.; Bischof, J. C. *Chem. Soc. Rev.* **2012**, *41*, 1191.
(54) Shao, J.; Xuan, M.; Dai, L.; Si, T.; Li, J.; He, Q. *Angew. Chem., Int. Ed.* **2015**, *54*, 12782.
(55) Govorov, A. O.; Richardson, H. H. *Nano Today* **2007**, *2*, 30.
(56) Merabia, S.; Shenogin, S.; Joly, L.; Keblinski, P.; Barrat, J. L. *Proc. Natl. Acad. Sci. U. S. A.* **2009**, *106*, 15113.
(57) Hinds, W. C. *Aerosol Technology: Properties, Behavior, and Measurement of Airborne Particles*; Wiley-VCH: Weinheim, 1999.
(58) Howse, J. R.; Jones, R. A. L.; Ryan, A. J.; Gough, T.; Vafabakhsh, R.; Golestanian, R. *Phys. Rev. Lett.* **2007**, *99*, 048102.

DOI: 10.1021/jacs.6b00902
J. Am. Chem. Soc. 2016, 138, 6492−6497